Dyes and Pigments 113 (2015) 145–150

Contents lists available at ScienceDirect

Dyes and Pigments

journal homepage: www.elsevier.com/locate/dyepig

A comparative study of peripheral and non-peripheral zinc (II) phthalocyanines incorporated into mesoporous silica nanoparticles

N.C. López Zeballos [a], M.C. García Vior [b], J. Awruch [b], L.E. Dicelio [a, *]

[a] INQUIMAE, Facultad de Ciencias Exactas y Naturales, Universidad de Buenos Aires, Ciudad Universitaria, Pabellón II, 1428 Buenos Aires, Argentina
[b] Departamento de Química Orgánica, Facultad de Farmacia y Bioquímica, Universidad de Buenos Aires, Junín 956, 1113 Buenos Aires, Argentina

ARTICLE INFO

Article history:
Received 4 June 2014
Received in revised form
28 July 2014
Accepted 4 August 2014
Available online 12 August 2014

Keywords:
Zinc(II) phthalocyanines
Mesoporous silica nanoparticles
Aggregation
Singlet oxygen
Fluorescence
Phthalocyanine release

ABSTRACT

The properties of two new lipophilic isomeric phthalocyanines 2,9(10),16(17),23(24)-tetrakis-[(2-dimethylamino)ethylsulfanyl]phthalocyaninatozinc(II) (**Pc9**) and 1,8(11),15(18),22(25)-tetrakis[(2-dimethylamino)ethylsulfanyl]phthalocyaninatozinc(II) (**Pc10**), incorporated into mesoporous silica nanoparticles were investigated. The photophysical studies showed that these dyes had a lower aggregation when incorporated into mesoporous silica nanoparticles than when incorporated into other carriers. Both systems were able to generate singlet oxygen, although with values lower than those obtained in homogeneous media, suggesting that a small portion of the phthalocynines was incorporated in an aggregated form. The incorporation efficiency determined by UV–Vis spectroscopy exceeded 99%.

A higher core release was obtained for the non-peripheral isomer (**Pc10**). This could be attributed to the steric hindrance effect of the substituents as compared with the peripheral substituted isomer (**Pc9**).

1. Introduction

Mesoporous silica nanoparticles (MSNs) have been shown to be efficient delivery carriers for biotechnological and biomedical applications [1]. Thus, different methods for the synthesis of silica-based nanoparticles have been described in the last years [2].

Hocine et al. described the synthesis of silicalites and MSNs, which covalently incorporate original water-soluble porphyrins for photodynamic therapy (PDT) applications. These authors performed PDT on MDAMB-231 breast cancer cells and found that all the nanoparticles showed significant cell death after irradiation. They attributed this to the singlet oxygen quantum yield (Φ_Δ) generation of the porphyrin-MSN [3].

Other authors reported that photosensitizer molecules such as HPPH [2-devinyl-2-(1-hexyloxyethyl)pyropheophorbide] [4] and PpIX (protoporphyrin IX) [5] are incorporated into organically modified silica (ORMOSIL) nanoparticles and that these molecules retain their spectroscopic and functional properties and could robustly generate cytotoxic singlet oxygen molecules upon photoirradiation.

Effective ways of trapping phthalocyanines inside porous silica have been reported elsewhere [6–8]. Also, the functionalization of silica nanoparticles with zinc phthalocyanine complexes tetra-substituted non-peripherally with 4-carboxyphenoxyl and 3-carboxyphenoxyl groups has been described. Phthalocyanine functionalized silica nanoparticles show higher fluorescence and triplet quantum yields as well as longer triplet lifetimes than free phthalocyanines [9].

A major difficulty in photobiological experiments is the poor solubility of the photosensitizer under physiological conditions. On the other hand, photosensitizer aggregation leads to a decrease in the photodynamic efficiency, which in turns limits the activity of the photosensitizer.

In the present study, we assessed the potential of MSNs as carriers for two novel zinc(II) lipophilic isomer phthalocyanines (ZnPc) synthesized in our laboratory: 2,9(10),16(17),23(24)-tetrakis-[(2-dimethylamino)ethylsulfanyl]phthalocyaninatozinc(II) (**Pc9**) and 1,8(11),15(18),22(25)-tetrakis[(2-dimethylamino)ethylsulfanyl] phthal-ocyaninatozinc(II) (**Pc10**), which have shown promising photobiological properties [10]. To this end, we investigated their incorporation into MSNs, their spectroscopic and photophysical properties, as well as their size and release.

2. Materials and methods

2.1. Chemical and reagents

Pc9 and **Pc10** [10] (Fig. 1) as well as tetra-*t*-butyl phthalocyaninatozinc(II) [11] were synthesized in our laboratory.

* Corresponding author. Tel.: +54 11 45763378; fax: +54 11 45763341.
E-mail addresses: led@qi.fcen.uba.ar, lelia.dicelio@gmail.com (L.E. Dicelio).

http://dx.doi.org/10.1016/j.dyepig.2014.08.004
0143-7208/

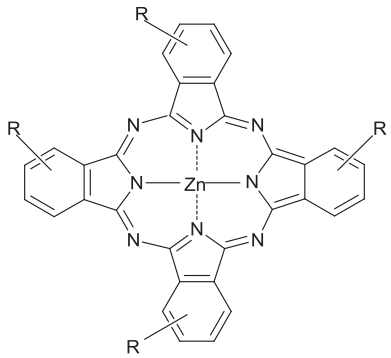

Pc9=**Pc10**; **R**= $SCH_2CH_2N(CH_3)_2$

Fig. 1. Chemical structure of phthalocyanines.

Cetyltrimethylammonium bromide (CTAB) was purchased from Merck (Germany), Tetraethylorthosilicate (TEOS) from Sigma–Aldrich (Steinheim, Germany), Imidazole BioUltra and Methylene Blue Hydrate (MB) from Fluka (Sigma–Aldrich, India), N,N-Diethyl-4-nitrosoaniline 97%, chloroform, ethyl acetate and tetrahydrofuran (THF) spectrophotometric grade from Sigma–Aldrich (Steinheim, Germany), HEPES BioUltra, for molecular biology from Sigma–Aldrich Germany (Schnelldorf, Germany), Sodium chloride from Mallinckrodt (Phillipsburg, NJ, USA), and Ammonium chloride from Sigma–Aldrich (Germany). All chemicals were of reagent grade and used without further purification. Distilled water treated in a Milli-Q system (Millipore) was used.

2.2. Instrumentation

Electronic absorption spectra were determined with a Shimadzu UV-3101 PC spectrophotometer. Fluorescence spectra were monitored with a QuantaMaster Model QM-1 PTI spectrofluorometer. Scanning electron microscopy (SEM) mesoporous silica microsphere images were obtained on a Zeiss Supra 40 microscope. Infrared (IR) and attenuated total reflection Fourier transform infrared (ATR-FTIR) spectra were performed with a Perkin Elmer Spectrum One FT-IR spectrometer.

2.3. Preparation of ZnPc-loaded mesoporous silica nanoparticles (ZnPc-MSNs)

Chloroform (3 mL) was dispersed in a 20 mL aqueous solution containing 0.4 g CTAB, and after stirring vigorously, a homogeneous microemulsion was obtained [12]. After 30 min sonication at room temperature, the microemulsion was heated at 60 °C to remove the chloroform. Water (80 mL) was added, followed by the addition of ethyl acetate (10 mL) with continuous stirring. Then, TEOS (1 mL) was added, followed by a dropwise addition of aqueous ammonia solution (25 wt.%). The resultant was stirred overnight, sonicated for 30 min and stirred again overnight at 40 °C. After centrifugation the precipitate was washed with ethanol and then with an ammonium nitrate solution (10 mg/mL). Ethanol was evaporated *in vacuo*, and HEPES buffer pH 7.4 145 mM NaCl (10 mL) was added to resuspend the MSNs.

To synthesize the ZnPc-MSNs, either **Pc9** or **Pc10** was dissolved in chloroform to obtain a concentration of 1.8×10^{-4} M, following the same procedure as above. Instead of water, HEPES buffer was added to each preparation.

2.3.1. Determination of incorporation efficiency (IE)

The IE was determined using UV spectroscopy. For that purpose the absorbance of the ZnPc at λ_{max} of the supernatant and washings after the incorporation of the ZnPc into the MSNs was subtracted from the starting concentration solution of the ZnPc to determine the concentration of the dye incorporated into the MSNs.

2.4. Characterization of ZnPc-MSN

2.4.1. Scanning electron microscopy

The morphology of ZnPc-MSNs was studied using SEM. To this end, the samples were seeded dropwise over a silicon wafer.

2.5. Photophysical parameters

2.5.1. Spectroscopic studies

The absorption and emission spectra of the two ZnPc-MSNs were recorded at room temperature with a 300 μL and 500 μL 10 × 10 mm quartz cuvette respectively. The emission spectra of the ZnPc-MSNs were collected at an excitation wavelength of 610 nm (Q-band) and recorded between 630 and 800 nm.

The optical spectra and absorbed photon flow for scattering media were recorded on a Shimadzu UV-3101 PC spectrophotometer fitted with an integrating sphere. $BaSO_4$ was used as a white standard to adjust the 100% reflectance level. The absorbance spectra were recorded for samples with dyes (A_2) and for MSNs free of dyes (A_1) according to the geometry recommended by Lagorio [13,14]. The real absorbance spectra of the dyes were calculated according to Eq. (1) which represents the dye absorbance without taking into account the contribution of the support.

$$A = -\log\left(1 - \frac{10^{-A_1} - 10^{-A_2}}{2}\right) \quad (1)$$

2.5.2. Fluorescence quantum yields

Fluorescence quantum yields (Φ_F) of the doped samples were determined by comparison with tetra-*t*-butyl phthalocyaninato-zinc(II) ($\Phi_F = 0.30$ in toluene [11]) as a reference at $\lambda_{exc} = 610$ nm. The calculation was performed as described elsewhere [11].

2.5.3. Quantum yield of singlet oxygen production

The quantum yield of singlet oxygen generation rates (Φ_Δ) was calculated by means of standard chemical monitor bleaching rates [15]. Imidazol (8 mM) and N,N-diethyl-4-nitrosoaniline (40–50 μM) in HEPES buffer were used for ZnPc-MSNs as a singlet oxygen chemical quencher [16]. The bleaching of nitrosoaniline was followed spectrophotometrically at 440 nm as a function of time. Polychromatic irradiation was performed using a projector lamp (Philips 7748SEHJ, 24V-250W), and a cut-off filter at 610 nm (Schott, RG 610) and a water filter were used to prevent infrared radiation. Both the ZnPc-MSNs and references (MB: $\Phi_\Delta = 0.56$ in HEPES buffer [15]) were irradiated within the same wavelength interval λ_1–λ_2, and Φ_Δ was calculated according to Ref. [14].

2.5.4. Aggregation studies of ZnPc-MSNs

The intensity absorption ratio of the two bands corresponding to the monomer and oligomers was calculated. The higher values of the ratio indicated a disaggregated dye form [17,18]. This ratio was calculated for all ZnPc-MSNs by using the λ_{max} indicated in Table 2. These values were compared with those obtained in THF, where no aggregation was observed.

2.5.5. Infrared spectroscopy

2.5.5.1. Fourier transform infrared spectroscopy (FT-IR). IR spectra of the nanoparticles were collected in transmission mode by pressing

Table 1
Particle size of MSNs and ZnPc-MSNs.

	MSN/nm	**Pc9**-MSN/nm	**Pc10**-MSN/nm
Average diameter	186.4 ± 57.76	194.17 ± 53.07	242.36 ± 39.80
Shell thickness	55.27 ± 6.51	49.30 ± 10.00	39.80 ± 11.12
Pore diameter	9.40 ± 3.30	14.20 ± 5.80	12.61 ± 4.52

Table 2
Monomer-dimer ratio of ZnPc in homogeneous media and MSNs.

	Pc9 THF	**Pc9**-MSN	**Pc9** HEPES	**Pc10** THF	**Pc10**-MSN	**Pc10** HEPES
Monomer/dimer ratio	6.094	1.655	0.533	5.686	1.908	0.942

the particle sample with KBr powder to form pellets. A resolution of 4 cm^{-1} and a total of 128 scans were applied for the collection of IR spectra [19].

2.5.5.2. Attenuated total reflectance-Fourier transform infrared spectroscopy (ATR-FTIR). ATR-FTIR spectra were collected by a Nicolet 8700 FTIR spectrophotometer connected to a fitting reflection horizontal ATR single crystal diamond. A total of 128 scans were performed for each spectrum and the resolution was 4 cm^{-1}. The software used to process the data was OMNIC version 7.3 (Thermo Electron Corporation).

2.5.6. Release studies in HEPES

An aliquot of 2 mL of ZnPc-MSNs was redispersed in 50 mL of HEPES buffer pH 7.4. Every 5 min, 500 μL was taken and replaced by the same amount of fresh buffer to keep the volume constant. After centrifugation of each aliquot, the concentration of the supernatant ZnPc was established by absorption spectroscopy. The values for the ZnPc released are the average of three determinations [12,20].

3. Results and discussion

3.1. Particle size distribution and morphology

Fig. 2 shows the microstructure and morphology of nanoparticles. All nanoparticles possessed a hollow core and a porous shell. The nanoparticles had an average size of 200 nm. The smallest one did not contain photosensitizer. The pore size was lower in the MSNs and the shell was thicker on the empty nanoparticles (Table 1). The difference of 48 nm in diameter of both ZnPc-MSNs could be attributed to the position of the substituents on the phthalocyanine macrocycle.

3.2. IR studies

Fig. 3 shows the FT-IR spectra of the ZnPc-MSNs. Bands observed at 1078 cm^{-1} correspond to Si—O, bands observed at 1090 and 800 cm^{-1} correspond to the Si—O—Si stretching and the band at 1637 cm^{-1} to the vibrations of the silica network and the OH stretching. Fig. 4 shows the spectra using ATR-FTIR where the shifts of the bands between the empty and loaded nanoparticles were more accentuated than in KBr.

3.3. Photophysical parameters

3.3.1. Absorption spectra and aggregation studies

Fig. 5 shows the absorbance spectra of the ZnPc in a homogeneous (THF) and a microheterogeneous (MSN) medium. The Q-band of the non-peripheral substituted phthalocyanine (**Pc10**)

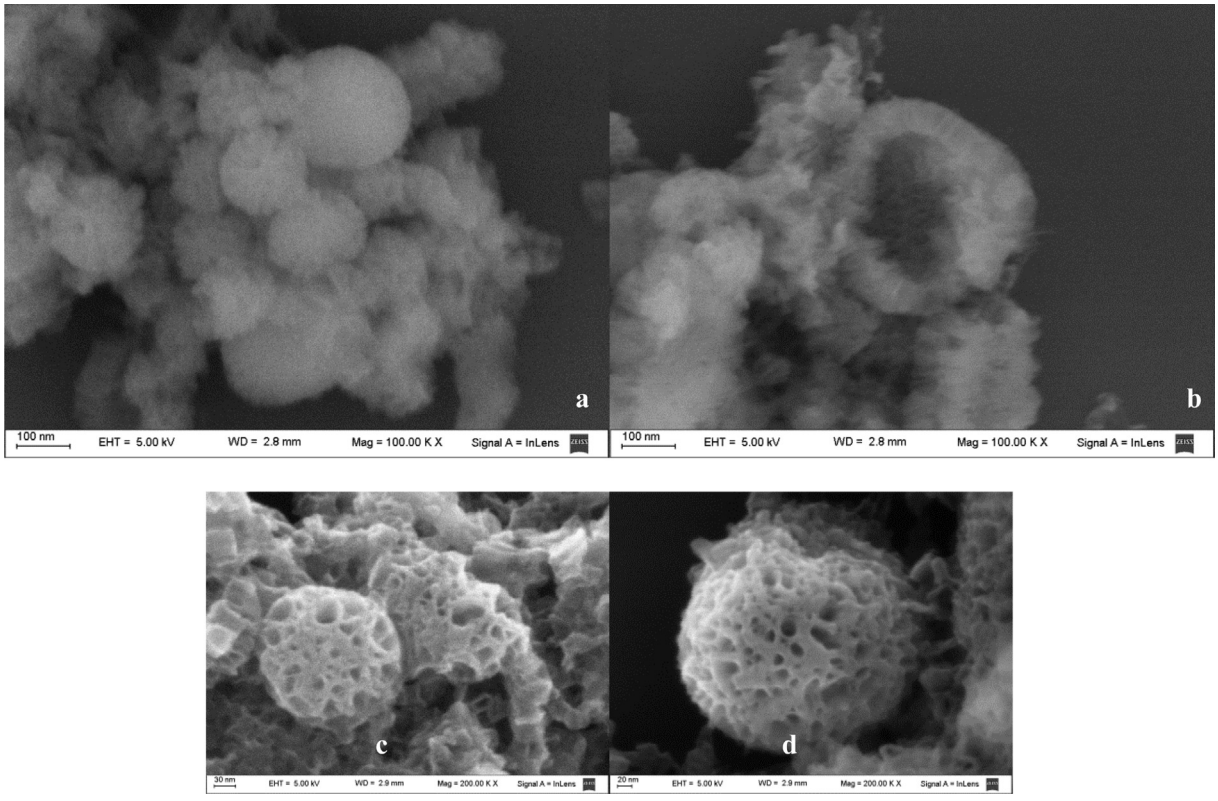

Fig. 2. SEM images; empty nanoparticles (a) and (b). **Pc9**-MSN (c), **Pc10**-MSN (d).

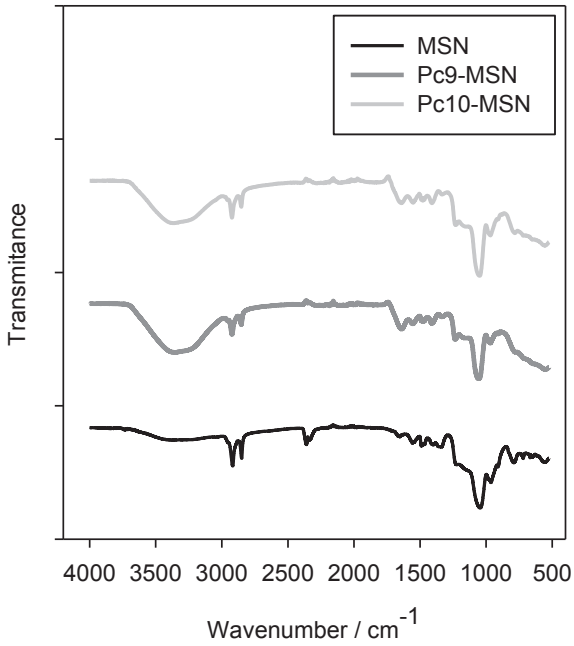

Fig. 3. IR spectra of MSN, **Pc9**-MSN and **Pc10**-MSN.

lies at a longer wavelength than that of the peripheral substituted phthalocyanine (**Pc9**), this behavior was observed both in homogeneous media [10] and MSN. The shape of the spectra of ZnPc-MSNs was similar to that of other zinc (II) phthalocyanines in organic solvents and liposomes. The spectra in Fig. 5 show a broad band and a new Q band in the 640–660 nm range, corresponding to a dimer-oligomer for **Pc9** and **Pc10**. The shape of the spectra of **Pc9**-MSN and **Pc10**-MSN showed an intermediate behavior between a hydrophilic and a lipophilic environment [21]. Furthermore, the peak intensity of the dimer-oligomer of **Pc9**-MSN and **Pc10**-MSN was higher than in the homogeneous medium, indicating that the dyes were aggregated. However, the monomer/oligomer values observed in **Pc9**-MSN and **Pc10**-MSN were approximately three and two times higher than those observed in HEPES indicating a lower aggregation behavior for the ZnPc-MSNs (Table 2). Furthermore, the tendency of aggregation in homogeneous media is higher in **Pc9** than in **Pc10**. The same behavior was

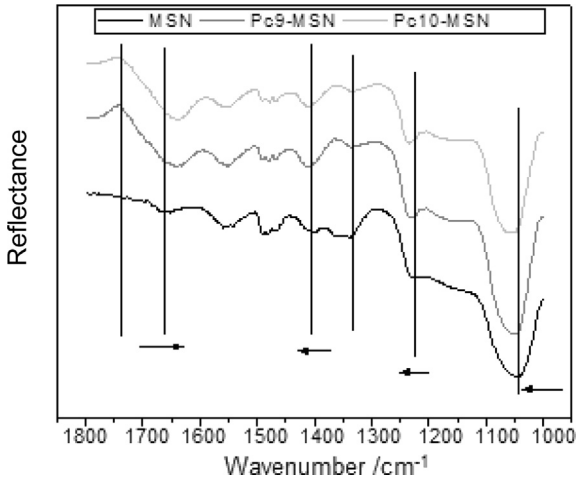

Fig. 4. ATR-FTIR spectra of MSN, **Pc9**-MSN and **Pc10**-MSN.

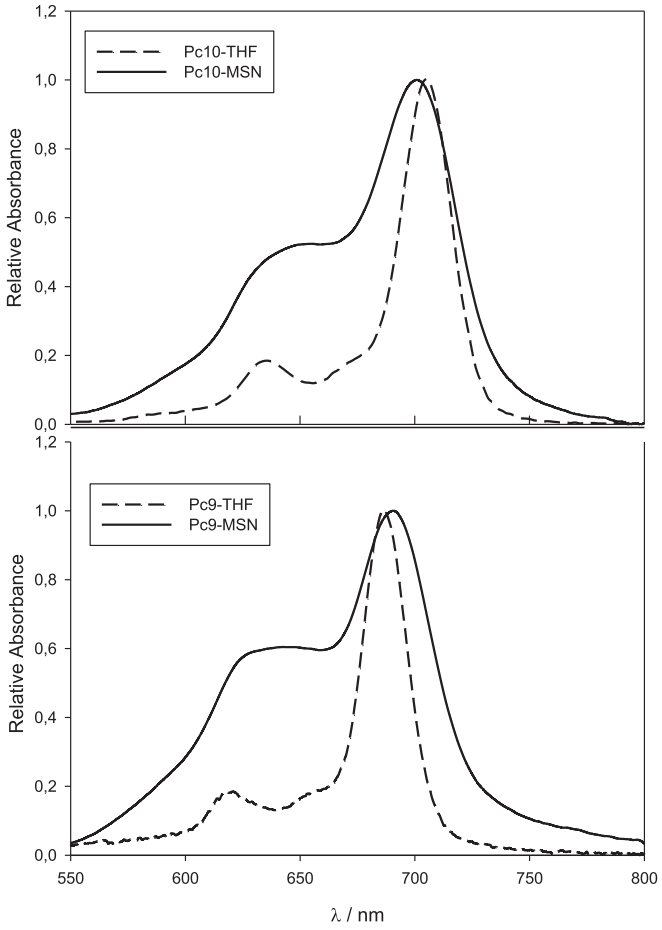

Fig. 5. Relative absorbance spectra.

observed for the incorporated dyes into the mesoporous nanoparticles.

3.3.2. *Fluorescence spectra*

The fluorescence emission spectra of phthalocyanines incorporated into MSNs are shown in Fig. 6. For both phthalocyanines, in solution and in mesoporous silica nanoparticles, no relevant modifications in spectral shape were observed indicating that the fluorescence can be attributed to monomers alone. However, the inner filter effects are a source of distortion of luminescence spectra and lowering of observed luminescence quantum yields and red shifts.

It was established that there are two kinds of interaction of monomers adsorbed on a solid: i) a strong interaction among coplanar ground state monomers leading to the formation of non-fluorescent dimers and ii) a weaker interaction among excited monomers and ground state neighboring molecules. The last interaction stabilizes excited monomers leading to a concentration dependent Stokes shift and accounts for the red shift obtained in the fluorescence spectra of samples where no re-absorption takes place [22].

3.3.3. *Fluorescence and singlet oxygen quantum yields*

When the phthalocyanines were incorporated into the nanoparticles, the values of Φ_F and Φ_Δ decreased as compared with the values obtained in THF (Table 3). This decrease was due to the aggregation effect and the non-radiative energy transfer to the

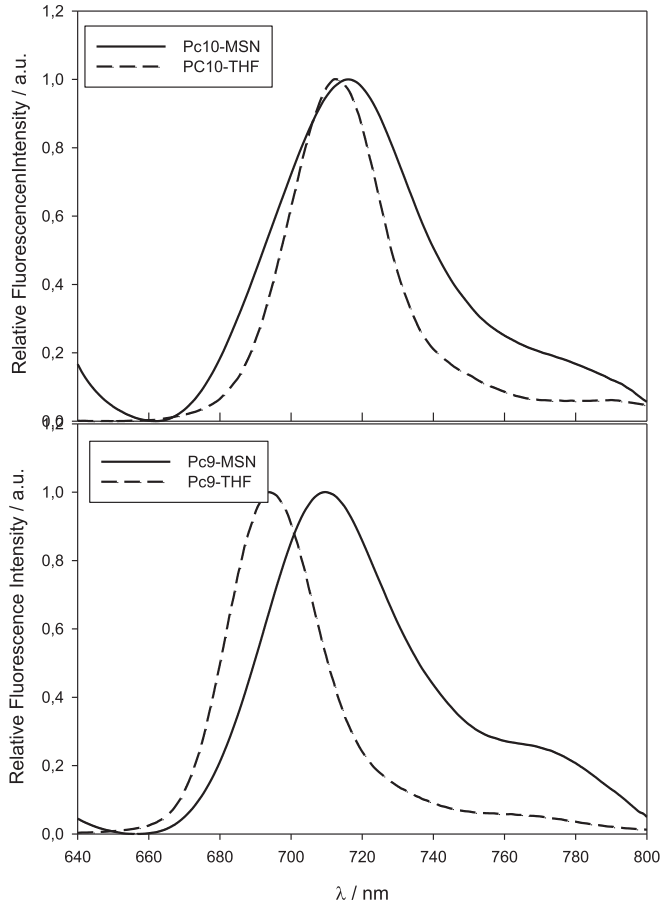

Fig. 6. Relative fluorescence intensity spectra.

environment. However, these values were higher than those obtained for other ZnPc incorporated into liposomes [20,21].

3.4. Determination of incorporation efficiency (IE)

The ZnPc were incorporated in the MSNs as described in section 2.3. Both dyes were incorporated with an efficiency higher than 99% (Table 3).

3.5. Determination of ZnPc release

The amount of ZnPc released from the MSNs is shown in Fig. 7, which shows the existence of two slopes for each ZnPc-MSN. The first slope would correspond to the release of the ZnPc, housed on the nanoparticle shell, while the second slope could be related to the release of the ZnPc located in the center of the MSN. The first slope is the same for both ZnPc-MSNs. The second slope shows the

Table 3
Spectral, and photophysical parameters in homogeneous media and in MSNs, and incorporation efficiency of ZnPc into MSNs.

Photophysical parameters	**Pc9**-THF[a]	**Pc9**-MSN	**Pc10**-THF[a]	**Pc10**-MSN
$\lambda_{max\ abs}$/nm	688	690	706	704
$\lambda_{max\ em}$/nm	694	710	712	716
Φ_F	0.28	0.014	0.18	0.017
Φ_Δ	0.60	0.42	0.73	0.39
IE/%	–	99.66	–	99.45

[a] Ref. [8].

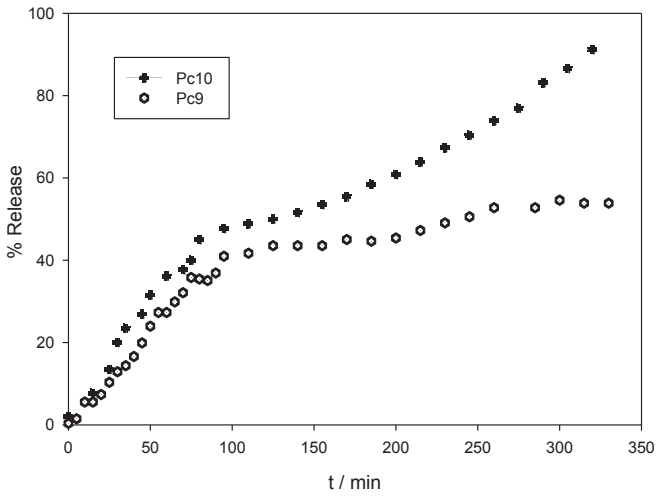

Fig. 7. Percentage release of phthalocyanines.

existence of a higher release for **Pc10** which could be attributed to the position and/or structure of the substituents on the macrocycle. According to this, we observed that the time of 50% release of the peripheral (β) substituted phthalocyanine (**Pc9**) was 245 min, while the time of the 50% release of the non-peripheral (α) phthalocyanine (**Pc10**) was 125 min. The same release profile has been previously obtained for another peripheral substituted ZnPc, 2,9(10),16(17),23(24)-tetrakis-(1-adamantylsulfanyl)phthalocyaninatozinc(II) [23] (unpublished data). As the adamantylsulfanyl group is a bulky-rigid substituent while 2-dimethylamino ethylsulfanyl group is only a bulky one the higher release for Pc10 could be attributed to the position and not the structure of substituents.

4. Conclusions

In this work MSNs with and without phthalocyanines with sizes of approximately 200 nm were synthesized.

The concentration of the dyes, approximately in the range of 10^{-4} M, resulted in a high percentage of incorporation. The photophysical studies showed a lower aggregation for these dyes when incorporated into MSNs than when incorporated into other carriers.

FTIR spectroscopy was used to confirm the existence of phthalocyanines in the silica network, whereas ATR-FTIR spectroscopy was used as support where the bands are more accentuated than in KBr.

Both ZnPc-MSNs were able to generate singlet oxygen. However, the lower Φ_Δ values compared to those obtained in homogeneous media, suggest that a small portion of the ZnPc-MSNs was incorporated in an aggregate form. The lower efficiency of the photoproduction of singlet oxygen is due not only to the presence of dimers, but also to the interaction between the dye and the silicon network surrounds.

A higher core release was obtained for the non-periperal isomer (**Pc10**) which could be attributed to the steric hindrance effect of the substituents as compared with the peripheral substituted isomer (**Pc9**).

Acknowledgments

This work was supported by grants from the University of Buenos Aires, and the Consejo Nacional de Investigaciones Científicas y Técnicas (CONICET), Argentina. We also wish to thank the language supervision by Mrs María Victoria Gonzalez Eusevi.

References

[1] Slowing II, Vivero-Escoto JL, Wu CW, Lin VSY. Mesoporous silica nanoparticles as controlled release drug delivery and gene transfection carriers. Adv Drug Deliv Rev 2008;60:1278–88.

[2] Couleaud P, Morosini V, Frochot C, Richeter S, Raehm L, Durand JO. Silica-based nanoparticles for photodynamic therapy applications. Nanoscale 2010;2:1083–95.

[3] Hocine O, Gary-Bobo M, Brevet D, Maynadier M, Fontaneld S, Raehm L, et al. Silicalites and mesoporous silica nanoparticles for photodynamic therapy. Int J Pharm 2010;402:221–30.

[4] Tymish Y, Ohulchanskyy TY, Roy I, Goswami NL, Chen Y, Bergey EJ, et al. Organically modified silica nanoparticles with covalently incorporated photosensitizer for photodynamic therapy of cancer. Nano Lett 2007;7:2835–42.

[5] Wang JQD, Cai F, Zhan Q, Wang Y, He S. Photosensitizer encapsulated organically modified silica nanoparticles for direct two-photon photodynamic therapy and in vivo functional imaging. Biomater 2012;33:4851–60.

[6] González-Santiago B, de la Luz V, Coahuila-Hernández MI, Rojas F, Tello-Solís SR, Campero A, et al. In situ physical or covalent trapping of phthalocyanine macrocycles within porous silica networks. Polyhedron 2011;30:1318–23.

[7] García-Sánchez MA, Quiroz-Segoviano RIY, Diaz-Alejo LA, Rojas F, Tello-Solís SR, Murguía-Cortéz L, et al. Cavity design via entrapment of tetrapyrrole macrocycles in sol-gel matrices for catalytic, optical, or sensoring functions. Adsorpt Sci Technol 2012;30:713–28.

[8] García-Sánchez MA, Rojas-González F, Menchaca-Campos EC, Tello-Solís SR, Quiroz-Segoviano RIY, Díaz-Alejo LA, et al. Crossed and linked histories of tetrapyrrolic macrocycles and their use for engineering pores within sol-gel matrices. Molecules 2013;18:588–653.

[9] Fascina A, Antunes E, Nyokong T. Characterization and photophysical behavior of phthalocyanines when grafted onto silica nanoparticles. Polyhedron 2013;53:278–85.

[10] Marino J, Garcia Vior MC, Dicelio LE, Roguin LP, Awruch J. Photodynamic effects of isosteric water-soluble phthalocyanines on human nasopharynx KB carcinoma cells. E. U J Med Chem 2010;45:4129–39.

[11] Fernández DA, Awruch J, Dicelio LE. Photophysical and aggregation studies of *t*-butyl substituted Zn phthalocyanines. Photochem Photobiol 1996;63:784–92.

[12] Liu C, Guo J, Yang W, Hu J, Wang C, Fu S. Magnetic mesoporous silica microspheres with thermo-sensitive polymer shell for controlled drug release. J Mater Chem 2009;19:4764–70.

[13] Lagorio MG. Reflectance spectroscopy using wine bottle glass. J Chem Educ 1999;76:1551–4.

[14] Amore S, Lagorio MG, Dicelio LE, San Roman E. Photophysical properties of supported dyes. Quantum yield calculations in scattering media. Prog React Kinet Mech 2001;26:159–77.

[15] Wilkinson F, Herman WP, Rose AD. Rate constant for the decay and reactions of the lowest electronically excited singlet state of molecular oxygen in solution. An expanded and revised compilation. J Phys Chem Ref Data 1995;24:663–1021.

[16] Kraljic I, El Mohsni S. A new method for the detection of singlet oxygen in aqueous solutions. Photochem Photobiol 1978;28:577–81.

[17] Alarcón E, Edwards AM, Garcia AM, Muñoz M, Aspée A, Borsarelli CD, et al. Photophysics and photochemistry of zinc phthalocyanine/bovine serum albumin adducts. Photochem. Photobiol Sci 2009;8:255–63.

[18] Rodríguez ME, Fernández DA, Awruch J, Braslavsky S, Dicelio LE. Effect of aggregation of a cationic phthalocyanine in micelles and in the presence of human serum albumin. J Porphyrins Phthalocyanines 2006;10:33–42.

[19] Li YS, Church JS, Woodhead AL, Moussa F. Preparation and characterization of silica coated iron oxide magnetic nano-particles. Spectrochim Acta Part A Mol Biomol Spectrosc 2010;76:484–9.

[20] López Zeballos NC, Marino J, García Vior MC, Chiarante N, Roguin LP, Awruch J, et al. Photophysics and photobiology of novel liposomal formulations of 2,9(10),16(17),23(24)-tetrakis[(2-dimethylamino)ethylsulfanyl]phthalocyaninato-zinc(II). Dyes Pigment 2013;96:626–35.

[21] Rodriguez ME, Morán F, Bonansea A, Monetti M, Fernández DA, Strassert CA, et al. A comparative study of photophysical and phototoxic properties of a new octaalkyl zinc (II) phthalocyanine incorporated in an hydrophilic polymer, in liposomes and in non ionic micelles. Photochem Photobiol Sci 2003;2:988–94.

[22] Lagorio MG, Dicelio LE, Litter MI, San Roman EA. Modeling of fluorescence quantum yields of supported dyes: aluminium carboxyphthalocyanine on cellulose. J Chem Soc Faraday Trans 1998;94:419–25.

[23] García Vior MC, Dicelio LE, Awruch J. Synthesis and properties of phthalocyanine zinc(II) complexes replaced with oxygen and sulfur linked adamantane moieties. Dyes Pigments 2009;83:375–80.